

---

# AGBD: A Global-scale Biomass Dataset

---

GhJulia Sialelli<sup>1</sup>    Torben Peters<sup>1</sup>    Jan D. Wegner<sup>2</sup>    Konrad Schindler<sup>1</sup>

<sup>1</sup>Photogrammetry and Remote Sensing, ETH Zurich

<sup>2</sup>EcoVision Lab, DM3L, University of Zurich

{gsialelli, tpeters, schindler}@ethz.ch

jandirk.wegner@uzh.ch

## Abstract

Accurate estimates of Above Ground Biomass (AGB) are essential in addressing two of humanity’s biggest challenges, climate change and biodiversity loss. Existing datasets for AGB estimation from satellite imagery are limited. Either they focus on specific, local regions at high resolution, or they offer global coverage at low resolution. There is a need for a machine learning-ready, globally representative, high-resolution benchmark. Our findings indicate significant variability in biomass estimates across different vegetation types, emphasizing the necessity for a dataset that accurately captures global diversity. To address these gaps, we introduce a comprehensive new dataset that is globally distributed, covers a range of vegetation types, and spans several years. This dataset combines AGB reference data from the GEDI mission with data from Sentinel-2 and PALSAR-2 imagery. Additionally, it includes pre-processed high-level features such as a dense canopy height map, an elevation map, and a land-cover classification map. We also produce a dense, high-resolution (10 m) map of AGB predictions for the entire area covered by the dataset. Rigorously tested, our dataset is accompanied by several benchmark models and is publicly available. It can be easily accessed using a single line of code, offering a solid basis for efforts towards global AGB estimation. The GitHub repository [github.com/ghjuliasialelli/AGBD](https://github.com/ghjuliasialelli/AGBD) serves as a one-stop shop for all code and data.

## 1 Introduction

Measuring Above Ground Biomass (AGB) is a crucial capability to combat biodiversity loss and address the ongoing climate crisis. Accurate AGB estimates enable the quantification of carbon stocks, which play a pivotal role in carbon offsetting schemes. Furthermore, AGB is correlated with various biodiversity metrics, providing valuable insights into the structure of biodiversity hotspots [1–3]. Traditional methods for measuring AGB are based on field work, either via destructive sampling, where sample trees are cut and weighed; or with non-destructive techniques that use tree dimensions (like tree height and trunk diameter at breast height) in tailored regression equations. Increasingly, LiDAR campaigns are replacing manual measurements with remote sensing, becoming the preferred method. However, despite their precision, the high costs and time requirements limit their global scalability. As a result, previous work has mainly focused on localized biomass estimation. Launched in 2019, the NASA GEDI mission uses an on-orbit laser altimeter aboard the International Space Station to scan the globe between 51.6° north and south. Calibrated on coincident airborne LiDAR data and ground plot field inventories, the mission provides sparse AGB estimates across its observation domain. These estimates represent the largest existing reference AGB dataset, which can be combined with Machine Learning (ML) methods and Remote Sensing (RS) data to advance

AGB estimation across the globe. We provide a ML-ready dataset consisting of coincident GEDI AGB estimates and various RS data products. Although freely accessible, obtaining remotely sensed data globally is tedious, and the sheer scale of it is prohibitive for ML research. The corresponding global dataset would require approximately 70TB of storage,  $\approx 60$  times more than the complete ImageNet. For biomass estimation that data will need extensive preprocessing, and it would be too large to repeatedly train and test within reasonable time during method development. To reduce the scale, but to the greatest possible extent maintain the representativeness of the dataset, we derive a subset of regions whose vegetation distribution emulates the global one. The complex interactions between AGB and various vegetation types [4] motivate this choice.

The dataset serves multiple purposes. (i) **Providing a globally representative high-res testbed for AGB estimation:** We show that all existing datasets are either too localized to generalize around the globe, or have only low resolution. Our collection covers all biomes and is globally representative at high resolution, enabling the training of AGB estimation models with improved performance and better generalization abilities. (ii) **Improving Regional Performance:** Prior research has shown that combining GEDI data with local reference data yields better results than using only the local data alone [5]. Researchers can leverage our comprehensive dataset for initial training and then fine-tune their models with local data specific to their regions, enhancing the accuracy and performance of their analyses.

To highlight the accessibility of our dataset, we offer a fully preprocessed version that is compatible with all major machine learning frameworks, such as TensorFlow and PyTorch. It is hosted on HuggingFace [6] and can be downloaded and used with just the following lines of code:

```
#!/pip install datasets
from datasets import load_dataset
dataset = load_dataset("prs-eth/AGBD", streaming=True)["train"] # or test, val
```

Our contributions are:

- We offer a machine learning-ready, easily accessible, globally representative dataset comprising coincident Aboveground Biomass (AGB) estimates together with various remote sensing data products.
- We conduct a comprehensive analysis of our dataset and apply several standard models to it to validate its accuracy and reliability and to serve as baselines.
- We generate and provide a dense, high-resolution (10 m) map of AGB predictions across the dataset's coverage area with the best-performing baseline.
- We release all benchmark models and pretrained weights.

All code is hosted on Github, moreover the original raw data, the dense predictions, and the model weights are hosted on the ETH Research Collection.

## 2 Background

In recent years, remote sensing (RS) and machine learning (ML) have advanced various mapping tasks, ranging from human population [7] to canopy height [8]. Biomass estimation also has seen significant research, with [9, 10] providing a review of existing AGB datasets and maps, supplemented in Table 1. Currently, global-scale AGB datasets suffer from low spatial resolution (at best 100 meters), while high-resolution datasets (10-30 meters) are limited to restricted geographic areas. This dichotomy forces researchers to strike a compromise between generalization across space and spatial resolution. Notably, [10] highlight the challenge of achieving consistent accuracy across continental and global-scale AGB maps, due to the absence of a comprehensive global reference

Table 1: Overview of existing work.

	<b>Method(s)</b>	<b>Geographical Extent</b>	<b>Resolution</b>	<b>Limitation</b>	<b>Reference data</b>	<b>Input data</b>
[12]	UNet	Finland	10m	Localized	NFI	S2, SAR
[16]	RF, SVM, CNN	Southwest China	10m	Localized	Destructive AGB measurements	S1, S2, SAR
[15]	RF	Northern Norway	10m	Localized	NFI	ArcticDEM, S2
[17]	UNet	Europe	30m	Localized	NFI	PlanetScope, LiDAR
[11]	CGAN	Northwestern USA	30m	Localized	LiDAR-derived maps	Landsat-8, ALOS-2 PALSAR-2
[18]	Maximum Entropy estimator	Democratic Republic of Congo	100m	Localized, low-resolution	LiDAR samples and allometry	Landsat, ALOS-2 PALSAR-2, SRTM
[19]	UNet	Vietnam, Myanmar	100m	Localized, low-resolution	ESA CCI Map	S2

dataset. Furthermore, [11] underscore the necessity for a dataset featuring globally distributed biomass reference records to improve regional studies. Similarly, [12] advocate for the release of more openly accessible, deep learning-ready data. [13] highlight another aspect of this issue when they apply a correction based on GEDI to their recent 1-meter resolution canopy height maps for São Paulo (Brazil) and California (USA), aiming to compensate for the limited geographic diversity of their reference data. Taken together, these observations point at a critical gap in the literature: there is a need for a robust, globally diverse dataset to support high-resolution AGB mapping.

In their comprehensive review of deep learning for remote sensing of forest inventories, [14] identify two critical avenues for progress. The first is the integration of data from multiple scales and sources, which has been shown to enhance predictive accuracy. For instance, incorporating diverse data modalities, such as DEM-derived Canopy Height Models (CHM) [15] and Synthetic Aperture Radar (SAR) data [16], not only alleviates issues of data saturation but also improves the predictive accuracy for high biomass values [9]. The second lever is the recognition and differentiation of various tree species, which can significantly refine the granularity and precision of forest inventory analyses. These strategies underscore the potential of deep learning to revolutionize forest monitoring and management through richer data integration and species-specific insights.

Our dataset fills in these gaps: it has a nominal resolution of 10 m, is representative of the global land cover and vegetation distribution, and assembles a range of data sources whose synergies have — to the best of our knowledge — not yet been systematically investigated for the task at hand.

### 3 Dataset

In this section, we discuss the rationale for creating the dataset, detail its components, and describe the process of its generation. For detailed information on data formats and downloading instructions, please refer to the supplementary material and the project website: [github.com/ghjuliasialelli/AGBD](https://github.com/ghjuliasialelli/AGBD).



Figure 1: The regions of interest: California (USA), Cuba, Austria, Greece, Nepal, Shaanxi (China), French Guiana, Paraguay, Ghana, Tanzania, New Zealand.

### 3.1 Vegetation types analysis

**Land Cover Classification Map (LC).** To correctly represent the world’s vegetation types, we turn to the Copernicus Global Land Service Dynamic Land Cover map [20], which delivers a global map of the land cover at 100 m spatial resolution. It consists of a discrete classification system with 21 classes (following UN-FAO’s Land Cover Classification System) that differentiates between open and closed forest types, with the following sub-types: evergreen needle-leaved (ENL), deciduous needle-leaved (DNL), evergreen broad-leaved (EBL), deciduous broad-leaved (DBL), mixed type, and unknown type. Additional land cover classes include shrubland, herbaceous vegetation, herbaceous wetland, moss and lichen, bare or sparse vegetation, cropland, built-up areas, snow and ice, and permanent water bodies. We refer the reader to [20] for detailed descriptions of each class. We base our analysis on the 2019 iteration of the product. Note that while the CGLS-LC100 map is global, we only consider vegetation types that are found within the GEDI coverage, as only there we have reference AGB data. As a consequence, vegetation types found only outside of the GEDI coverage are not accounted for. These are: open and closed DNL only found in Siberia; and moss and lichen, mostly found in Northern Canada, Siberia and Greenland.

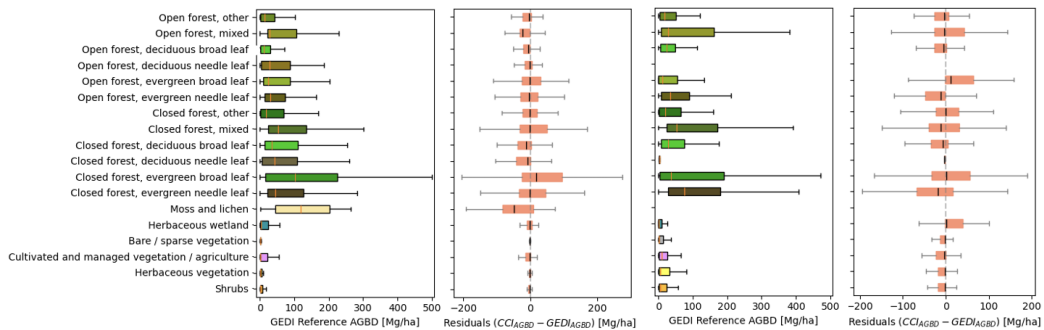


Figure 2: Per-biome distribution of GEDI AGBD values and CCI residuals. Left: global scale, Right: subset scale.

**A globally representative vegetation distribution.** The ESA CCI map is the most recent and adequate global AGB map available. It is provided by the European Space Agency (ESA), through its Climate Change Initiative (CCI) Biomass project. Global maps of AGB are provided for five epochs (2010, 2017, 2018, 2019 and 2020) at 100 m resolution. We observe that this map performs variably across different vegetation types, as shown in Figure 2. We utilise CCI AGB estimates and

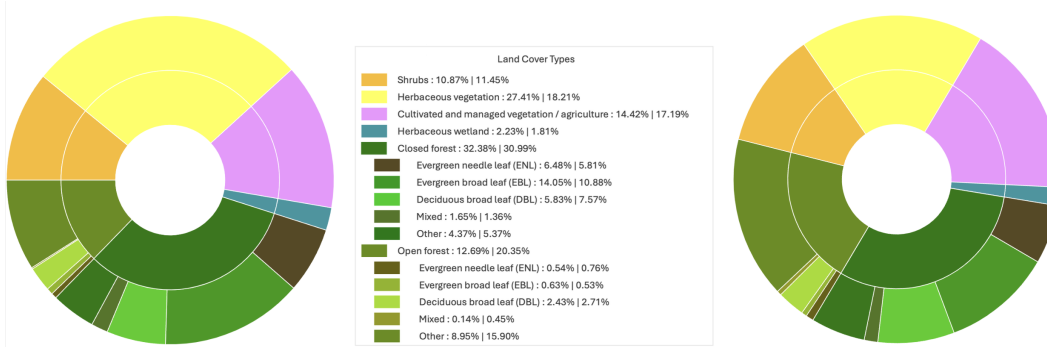


Figure 3: Land cover distribution across the world (left) and across our subset (right).

GEDI footprints from the year 2019 to analyze residuals across various vegetation types within the GEDI coverage. Our analysis revealed significant variances, with underestimations in moss and lichen and overestimations in closed evergreen broadleaf forests, compelling us to adopt a design that accounts for differences between vegetation types. In the absence of a truly global dataset and facing the logistical barrier of large-scale remote sensing data downloads, we argue for a reasonably-sized dataset that mirrors the global vegetation distribution. To that end we select the following regions: California (USA), Cuba, Austria, Greece, Nepal, Shaanxi (China), French Guiana, Paraguay, Ghana, Tanzania and New Zealand. They are strategically chosen for their geographic and ecological diversity, as illustrated in Figures 1 and 3. Both the vegetation types and the ESA CCI residuals within our subset are in fairly good agreement with the global ones (Figure 2).

### 3.2 Modalities

In the following we describe the data sources, how they were processed, and how we assembled them into the final dataset. The process is illustrated in fig. 4. A more detailed explanation of each individual data field can be found on the project website.

**GEDI**, an altimeter mission (2018-2023) on the International Space Station, produced high-resolution laser observations of the Earth’s 3D structure. It collected billions of cloud-free observations from 51.6°N to 51.6°S. We downloaded all GEDI L4A (v2.1) footprints for the regions of interest from the start of the mission until Dec. 31st 2020. We only kept biomass values in the range [0, 500] Mg/ha, as suggested by previous literature [21]; we only retain the "power" beams, as previous work [22, 23] has found that they provide more reliable estimates than the "coverage" beams; and as suggested by the GEDI team, we discard footprints where  $sensitivity < 0.95$ ,  $14\_quality\_flag \neq 1$ , and  $selected\_algorithm = 10$ .

**Sentinel-2 (S2)**, a European multi-spectral imaging mission, delivers high-resolution imagery with a revisit frequency of 5 days at the equator. We downloaded Level-1C products from PEPS, processed to Level-2A using Sen2Cor [24] (v2.11), and selected images with less than 20% cloud coverage from October 2018 to December 2020. The pre-processing of the products involves the conversion of raw digital numbers ( $DN$ ) to surface reflectance values via  $SR = \frac{DN + BOA\_offset}{10,000}$ , with  $BOA\_offset$  equal to 0 prior to January 2022, and  $-1000$  after that.

**PALSAR-2 (P2)**, on board the ALOS-2 satellite, is a Synthetic Aperture Radar (SAR) that can capture images at night and through clouds, making it a 24-hour, all-weather technology. The 25 m PALSAR-2 mosaic is a seamless global image in WGS84 (EPSG:4326) projection, created by merging strips of SAR imagery, featuring both HH and HV polarization backscatter. It uses a different gridding system from ESA, so for each year we download the necessary ALOS tiles, then mosaic, crop and reproject them to align with Sentinel-2 tiles. The provided digital numbers ( $DN$ ) are linear backscatter amplitudes. Pre-processing involves converting  $DN$  values to  $\gamma_0$  values in decibels via  $\gamma^0 = 10 \cdot \log_{10}(DN^2) - 83$ .

**Digital Elevation Model (DEM).** The ALOS Global Digital Surface Model (AW3D30) offers 30-meter resolution elevation data. As for the PALSAR-2 mosaic we downloaded, mosaicked, and reprojected the DEM to align with Sentinel-2 tiles.

**Land Cover (LC).** We downloaded the Copernicus Global Land Service Dynamic Land Cover map at 100-meter resolution, cropped and reprojected it to match Sentinel-2 tiles.

**Canopy Height (CH).** [8] provides source code for canopy height mapping from Sentinel-2 imagery, using probabilistic deep learning. The model estimates CH for each input Sentinel-2 L2A image and merges redundant predictions from different dates to create a yearly CH map for each Sentinel-2 tile, along with a map of the associated standard deviations (STD). We follow this procedure to obtain yearly CH maps for 2019 and 2020 for all Sentinel-2 tiles within our regions of interest.

### 3.3 Dataset Assembly and Train/Test Split

To create an analysis-ready dataset, we crop all data into patches as follows: first all data sources are upsampled to a uniform resolution of 10 m, using bilinear interpolation for continuous variables and nearest neighbor for categorical variables. We then iterate over all GEDI footprints within the area of interest, crop all raster data to  $25 \times 25$  pixel squares centered at the GEDI footprint, and store them in a HDF5 file. For more details please refer to the Appendix.

The splitting into training, validation and test sets is done not at the level of GEDI footprints but along Sentinel-2 tiles, meaning that all patches within the same  $100 \times 100 \text{ km}^2$  tile will belong to the same set. To align with our geographical distribution and vegetation types, we split each country/region into training, validation and test portions and aim to match the distribution of vegetation types within each portion to that of the whole region. To that end we randomly explore the combinatorial assignment of tiles to the three portions until a sufficiently close match has been found. In each region 65% of the tiles are used for training, 15% for validation, and the remaining 20% for testing. The detailed assignment per tile can be found on our project website.

## 4 Benchmark

### 4.1 Models

Early works on biomass estimation employed linear regression models, but the relationship between satellite observations and AGB is more complex and can be better modeled with high-capacity ML methods [16, 25]. We provide a suite of pertinent ML models as benchmarks for the task.

**GBDT.** We start with a `lightgbm` implementation of Gradient Boosted Decision Trees (GBDT). This model does not leverage the spatial context information of the patches but performs regression based only on the central pixel. The model was trained by minimising the RMSE loss, with early stopping enabled. Model hyper-parameters can be found in the Appendix.

For the following deep learning methods, we always use a patch-wise training procedure: each patch (of size  $2k + 1 \times 2k + 1$ ) has *one* ground-truth pixel, its center. The model emits a prediction for each pixel in the patch, but only the central pixel prediction contributes to the loss. The optimisation of the network parameters is done in the standard way with mini-batch stochastic gradient descent, using the ADAM [26] variant and batch size 256. Each model is trained five times with different random seeds to account for stochastic variability, and we always report the mean RMSE and standard deviation over the five runs. All models run on consumer hardware, specifically we used NVIDIA GeForce RTX 2080 Ti GPUs available through the ETH high-performance cluster. The training pipeline is illustrated in Figure 4.

**FCN (0.5M parameters).** This model is a straightforward Fully Convolutional Neural Network (FCN) consisting of convolutional layers with batch normalization and ReLU activations. The channel depth

increases as [32, 64, 128, 128, 128, 128]. Convolutional layers use a stride of 1 and padding of 1 to preserve spatial dimensions. The final convolution maps the 128 feature channels to a single output channel.

**UNet** (10M parameters). A standard UNet implementation with an initial double convolution block, followed by symmetric downsampling and upsampling layers with skip connections to preserve spatial detail, and a final output convolution to produce a single-channel output. The number of down- and up-sampling layers depends on the patch size, with larger patches going through more layers.

**Lang et al.** (13M parameters). The architecture developed in [8] for CH estimation, but trained with standard  $\ell_2$ -loss (rather than the original log-likelihood loss). It consists of a series of residual blocks with separable convolutions *without* any downsampling. For details, refer to [8].

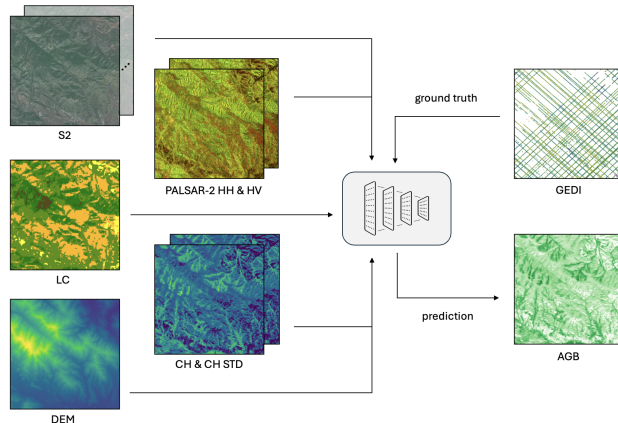


Figure 4: Visualization of all data sources (except geographic coordinates) along with our training pipeline. Note the sparse GEDI labels, which are upgraded to dense AGB maps by the prediction.

## 4.2 Results

All qualitative results are reported in Table 2. The lowest error is achieved with the architecture of Lang et al., trained on all considered input channels. The best models achieve RMSE values slightly below 60 Mg/ha, consistent with previous literature.

**Role of input features.** In order to study the impact of each data source, we conduct a series of experiments. We vary the input features available to each model and alternative feed: all features, only the canopy height (**CH**), only the 10 m RGB (B02, B03, B04) and NIR (B08) Sentinel-2 bands (**RGBN**), all Sentinel-2 bands (**S2 (all)**), all Sentinel-2 bands plus the LC map (**LC**), all Sentinel-2 bands plus the DEM (**DEM**), all Sentinel-2 bands plus the two ALOS-2 PALSAR-2 bands (**P2**), and features except for the CH. Per-pixel latitude and longitude are always provided as inputs. Each model is evaluated with every feature combination, and in each run the weights with the highest validation score are applied to the held-out test set to obtain the RMSE values reported in Table 2. Additionally we also show feature importance plots obtained with the GBDT model in the Appendix.

**Patch size.** To study how varying the patch-size affects model performance, we train and evaluate with two different patch sizes,  $15 \times 15$  and  $25 \times 25$  pixels, see Table 2.

**Binned residuals analysis.** Beyond overall test RMSE we also analyse the residual distribution across various AGB intervals, see Figure 6. Besides our baseline models described in Section 4.1 we also include the ESA CCI AGB map, upsampled to 10 m resolution, in this analysis. That comparison is directly relevant, since ESA CCI also uses GEDI to calibrate their model, according to their Algorithm Theoretical Basis Document [27, p.23]. We point out that the distribution of AGB values

is skewed: most (50%) of all GEDI labels fall into the first bin ( $[0, 50]$ ). Density scatter plots can be found in the Appendix.

**Qualitative results inspection.** For a visual impression, Figure 5 shows the predictions of the best-performing model versus the CCI maps for two Sentinel-2 tiles: one in Ghana (30NXM) and one in Paraguay (21KVQ).

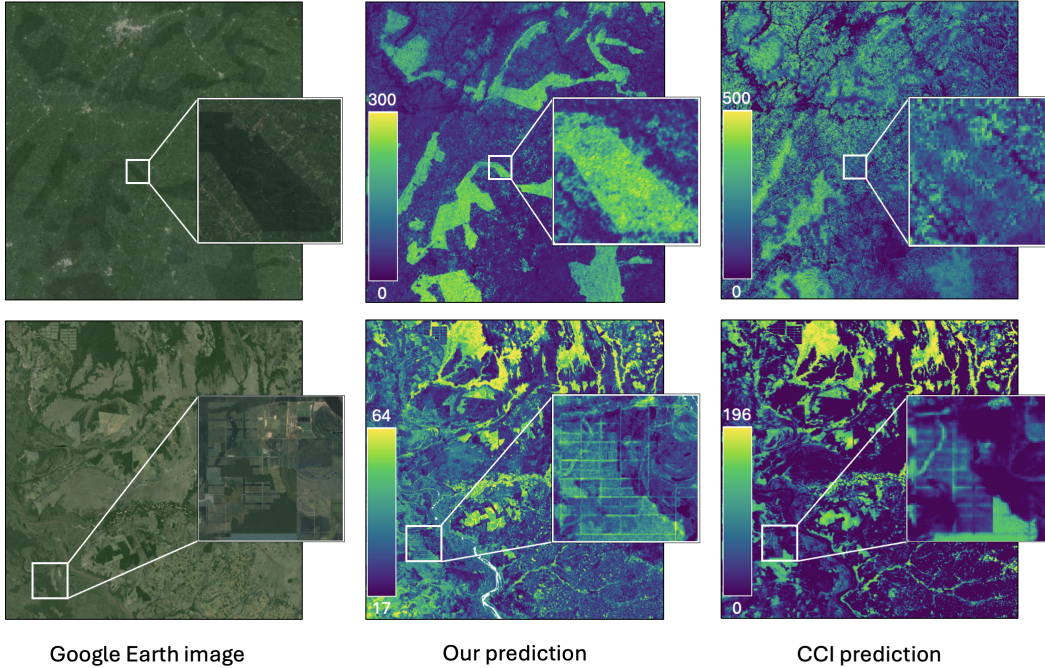


Figure 5: Maps predicted by the best model vs. ESA CCI maps, for two Sentinel-2 tiles: 30NXM (top) and 21KVQ (bottom). *Small offsets are due to Google Earth using a different map projection.*

Table 2: Mean test RMSE ( $\downarrow$ ) and associated standard deviation per model, with various inputs. Crosses denote the *presence* of a feature, values in brackets denote patch size. RMSE values in the lowest 10% of the range are colour-coded, with darker blue indicating better results.

Features						Methods							
CH	RGBN	S2 (all)	LC	DEM	P2	GBDT		FCN		UNet		Lang et al. [8]	
						(1×1)	(15×15)	(25×25)	(15×15)	(25×25)	(15×15)	(25×25)	
×						69.88 ±0.17	69.50 ±0.13	69.49 ±0.11	68.99 ±0.15	68.73 ±0.22	68.43 ±0.10	68.04 ±0.09	
	×					74.74 ±0.23	65.35 ±0.16	65.06 ±0.26	63.25 ±0.31	62.11 ±0.52	61.73 ±0.30	60.39 ±0.22	
			×			70.93 ±0.35	64.16 ±0.22	63.92 ±0.40	61.87 ±0.14	60.94 ±0.22	60.46 ±0.15	60.68 ±0.46	
				×		67.52 ±0.15	62.57 ±0.22	62.48 ±0.28	61.17 ±0.23	60.30 ±0.16	59.72 ±0.28	58.80 ±0.08	
					×	68.38 ±0.15	63.30 ±0.24	63.92 ±0.34	61.61 ±0.15	60.59 ±0.10	60.05 ±0.13	59.03 ±0.09	
					×	68.69 ±0.27	62.19 ±0.35	61.94 ±0.21	60.40 ±0.14	59.24 ±0.18	59.08 ±0.05	58.04 ±0.13	
			×	×	×	65.63 ±0.08	61.47 ±0.21	61.34 ±0.03	59.85 ±0.12	58.97 ±0.14	58.64 ±0.08	57.87 ±0.11	
×		×	×	×	×	63.64 ±0.06	61.29 ±0.13	61.22 ±0.27	60.02 ±0.18	59.20 ±0.14	58.67 ±0.08	58.16 ±0.19	

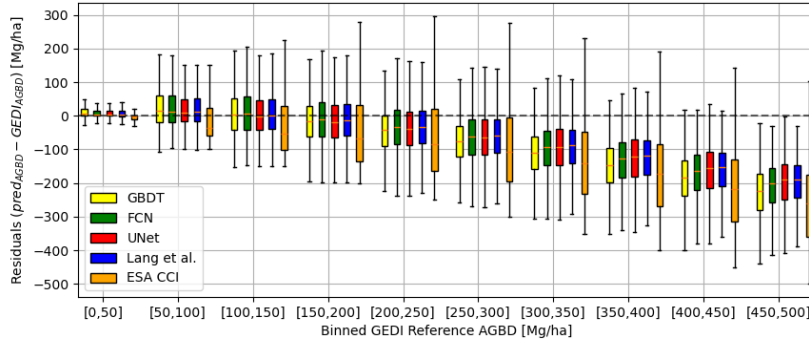


Figure 6: Binned residuals over the test set for the best-performing version of each architecture, and for the ESA CCI predictions.

## 5 Discussion

**Results.** The input features study confirms that including more input features is beneficial, and that models with more parameters tend to better capture the complex relationship between input features and AGB. The best result overall is achieved by the architecture of Lang et al., with a patch size of  $25 \times 25$  and all input channels. Thus, it makes sense to assemble a dataset with a wider range of observations. In particular the results underline that, while canopy height and biomass are strongly correlated, it is not straightforward to accurately derive the latter only from the former.

Figure 5 illustrates how the high spatial resolution of our estimates is able to preserve spatial details that are not captured in the CCI product, meaning that they would not be restored by conventional upscaling of existing maps. Given the limited spatial context of most existing biomass retrieval methods, it is interesting that increasing the context window yields better results. At present it is unclear whether this is due to real context information or simply a data augmentation effect. Consistent with the literature, the residuals analysis highlights the commonly observed under-estimation of higher biomass values, although the comparison to CCI suggests that our deep learning methods mitigate that effect.

**Limitations.** Despite the nominal 10 m resolution of our estimates, the effective spatial resolution at which biomass is identified is lower: we actually learn to predict, at each pixel, the highest biomass within a  $\approx 25\text{m}$  diameter (the size of the GEDI footprint). Another point to keep in mind is that the spatial distribution of GEDI footprints is not uniform: the sampling gets progressively denser as one approaches towards the borders of the observed region at  $\pm 51.6^\circ$ .

## 6 Conclusion

We provide a ML-ready, unrestricted, easily accessible dataset for high-resolution biomass estimation from remote sensing data. This dataset consists of  $\approx 16 \cdot 10^6$  patches, covering a diverse and representative selection of geographic locations with a total of  $\approx 500 \cdot 10^6$  hectares and two different years, 2019 and 2020. Furthermore, we complement the dataset with a suite of baseline architectures and trained weights for others to build upon. We hope that our dataset may help to reduce the geographical and ecosystem-related biases of biomass models, enhance the accuracy of future biomass maps, and perhaps contribute towards a regular, operational high-resolution monitoring system.

## 7 Acknowledgments

The data products used for this paper have been collected from various sources:

- the Global PALSAR-2/PALSAR/JERS-1 Mosaics and Forest/Non-Forest Maps of the Japan Aerospace Exploration Agency;
- the ALOS Global Digital Surface Model "ALOS World 3D - 30m (AW3D30)" of the Japan Aerospace Exploration Agency;
- the Land Cover 2019 (v3) of the European Union's Copernicus Land Monitoring Service;
- the Sentinel-2 L1C products, courtesy of Copernicus, downloaded via the French PEPS platform;
- the GEDI L4A product, courtesy of the NASA GEDI Team, downloaded from Oak Ridge National Laboratory DAAC.

We thank them for making this data openly available for academic purposes.

## References

- [1] Heather D. Vance-Chalcraft et al. "Relationship Between Aboveground Biomass and Multiple Measures of Biodiversity in Subtropical Forest of Puerto Rico". In: *Biotropica* 42.3 (May 2010), pp. 290–299. ISSN: 1744-7429. DOI: 10.1111/j.1744-7429.2009.00600.x. URL: <http://dx.doi.org/10.1111/j.1744-7429.2009.00600.x>.
- [2] Judit Sonkoly et al. "Both mass ratio effects and community diversity drive biomass production in a grassland experiment". In: *Scientific Reports* 9.1 (Feb. 2019). ISSN: 2045-2322. DOI: 10.1038/s41598-018-37190-6. URL: <http://dx.doi.org/10.1038/s41598-018-37190-6>.
- [3] Shuaifeng Li et al. "Positive relationship between species richness and aboveground biomass across forest strata in a primary Pinus Kesiya forest". In: *Scientific Reports* 8.1 (Feb. 2018). ISSN: 2045-2322. DOI: 10.1038/s41598-018-20165-y. URL: <http://dx.doi.org/10.1038/s41598-018-20165-y>.
- [4] Xia Chen, Mingyu Luo, and Markku Larjavaara. "Effects of climate and plant functional types on forest above-ground biomass accumulation". In: *Carbon Balance and Management* 18.1 (Mar. 2023). ISSN: 1750-0680. DOI: 10.1186/s13021-023-00225-1. URL: <http://dx.doi.org/10.1186/s13021-023-00225-1>.
- [5] Eric L Bullock et al. "Estimating aboveground biomass density using hybrid statistical inference with GEDI lidar data and Paraguay's national forest inventory". In: *Environmental Research Letters* 18.8 (July 2023), p. 085001. ISSN: 1748-9326. DOI: 10.1088/1748-9326/acdf03. URL: <http://dx.doi.org/10.1088/1748-9326/acdf03>.
- [6] Quentin Lhoest et al. "Datasets: A Community Library for Natural Language Processing". In: *Proceedings of the 2021 Conference on Empirical Methods in Natural Language Processing: System Demonstrations*. Online and Punta Cana, Dominican Republic: Association for Computational Linguistics, Nov. 2021, pp. 175–184. arXiv: 2109.02846 [cs.CL]. URL: <https://aclanthology.org/2021.emnlp-demo.21>.
- [7] Nando Metzger et al. *High-resolution Population Maps Derived from Sentinel-1 and Sentinel-2*. 2023. DOI: 10.48550/ARXIV.2311.14006. URL: <https://arxiv.org/abs/2311.14006>.
- [8] Nico Lang et al. "A high-resolution canopy height model of the Earth". In: *Nature Ecology & Evolution* 7.11 (Sept. 2023), pp. 1778–1789. ISSN: 2397-334X. DOI: 10.1038/s41559-023-02206-6. URL: <http://dx.doi.org/10.1038/s41559-023-02206-6>.
- [9] Yuzhen Zhang, Shunlin Liang, and Lu Yang. "A Review of Regional and Global Gridded Forest Biomass Datasets". In: *Remote Sensing* 11.23 (Nov. 2019), p. 2744. ISSN: 2072-4292. DOI: 10.3390/rs11232744. URL: <http://dx.doi.org/10.3390/rs11232744>.

- [10] Arnan Araza et al. “A comprehensive framework for assessing the accuracy and uncertainty of global above-ground biomass maps”. In: *Remote Sensing of Environment* 272 (Apr. 2022), p. 112917. ISSN: 0034-4257. DOI: 10.1016/j.rse.2022.112917. URL: <http://dx.doi.org/10.1016/j.rse.2022.112917>.
- [11] Johannes Leonhardt et al. “Probabilistic Biomass Estimation with Conditional Generative Adversarial Networks”. In: *Pattern Recognition*. Springer International Publishing, 2022, pp. 479–494. ISBN: 9783031167881. DOI: 10.1007/978-3-031-16788-1\_29. URL: [http://dx.doi.org/10.1007/978-3-031-16788-1\\_29](http://dx.doi.org/10.1007/978-3-031-16788-1_29).
- [12] Andrea Nascetti et al. “BioMassters: A Benchmark Dataset for Forest Biomass Estimation using Multi-modal Satellite Time-series”. In: *Advances in Neural Information Processing Systems* 36 (2024). URL: [https://papers.nips.cc/paper\\_files/paper/2023/file/40daf2a00278c4bea1b26cd4c8a654f8-Paper-Datasets\\_and\\_Benchmarks.pdf](https://papers.nips.cc/paper_files/paper/2023/file/40daf2a00278c4bea1b26cd4c8a654f8-Paper-Datasets_and_Benchmarks.pdf).
- [13] Jamie Tolan et al. “Very high resolution canopy height maps from RGB imagery using self-supervised vision transformer and convolutional decoder trained on aerial lidar”. In: *Remote Sensing of Environment* 300 (Jan. 2024), p. 113888. ISSN: 0034-4257. DOI: 10.1016/j.rse.2023.113888. URL: <http://dx.doi.org/10.1016/j.rse.2023.113888>.
- [14] Alireza Hamedianfar et al. “Deep learning for forest inventory and planning: a critical review on the remote sensing approaches so far and prospects for further applications”. In: *Forestry: An International Journal of Forest Research* 95.4 (Feb. 2022), pp. 451–465. ISSN: 1464-3626. DOI: 10.1093/forestry/cpac002. URL: <http://dx.doi.org/10.1093/forestry/cpac002>.
- [15] S. Puliti et al. “Modelling above-ground biomass stock over Norway using national forest inventory data with ArcticDEM and Sentinel-2 data”. In: *Remote Sensing of Environment* 236 (Jan. 2020), p. 111501. ISSN: 0034-4257. DOI: 10.1016/j.rse.2019.111501. URL: <http://dx.doi.org/10.1016/j.rse.2019.111501>.
- [16] Wenjun Liu et al. “Machine learning-based grassland aboveground biomass estimation and its response to climate variation in Southwest China”. In: *Frontiers in Ecology and Evolution* 11 (Mar. 2023). ISSN: 2296-701X. DOI: 10.3389/fevo.2023.1146850. URL: <http://dx.doi.org/10.3389/fevo.2023.1146850>.
- [17] Siyu Liu et al. “The overlooked contribution of trees outside forests to tree cover and woody biomass across Europe”. In: *Science Advances* 9.37 (Sept. 2023). ISSN: 2375-2548. DOI: 10.1126/sciadv.adh4097. URL: <http://dx.doi.org/10.1126/sciadv.adh4097>.
- [18] Liang Xu et al. “Spatial Distribution of Carbon Stored in Forests of the Democratic Republic of Congo”. In: *Scientific Reports* 7.1 (Nov. 2017). ISSN: 2045-2322. DOI: 10.1038/s41598-017-15050-z. URL: <http://dx.doi.org/10.1038/s41598-017-15050-z>.
- [19] Antonio Elia Pascarella et al. “ReUse: REgressive U-net for Carbon Storage and Above-Ground Biomass Estimation”. In: *Journal of Imaging* 9.3 (Mar. 2023), p. 61. ISSN: 2313-433X. DOI: 10.3390/jimaging9030061. URL: <http://dx.doi.org/10.3390/jimaging9030061>.
- [20] M. Buchhorn et al. *Copernicus Global Land Service: Land Cover 100m: Collection 3: epoch 2019: Globe (Version V3.0.1) [Data set]*. 2020. DOI: 10.5281/zenodo.3939050. URL: <https://zenodo.org/records/3939050>.
- [21] Joao Carreiras et al. “Coverage of high biomass forests by the ESA BIOMASS mission under defense restrictions”. In: *Remote Sensing of Environment* 196 (May 2017), pp. 154–162. DOI: 10.1016/j.rse.2017.05.003.
- [22] Clemence Lanfranchi et al. *Global Biomass Mapping and Uncertainty Estimation from GEDI LIDAR Data using Bayesian Deep Learning*. 2022. URL: [https://ethz.ch/content/dam/ethz/special-interest/baug/igp/photogrammetry-remote-sensing-dam/documents/pdf/Student\\_Theses/MA\\_ClemenceLanfranchi.pdf](https://ethz.ch/content/dam/ethz/special-interest/baug/igp/photogrammetry-remote-sensing-dam/documents/pdf/Student_Theses/MA_ClemenceLanfranchi.pdf).
- [23] Kamel Lahssini et al. “Influence of GEDI acquisition and processing parameters on canopy height estimates over tropical forests”. en. In: *Remote Sens. (Basel)* 14.24 (Dec. 2022), p. 6264.
- [24] Magdalena Main-Knorn et al. “Sen2Cor for Sentinel-2”. In: *Image and Signal Processing for Remote Sensing XXIII*. Ed. by Lorenzo Bruzzone, Francesca Bovolo, and Jon Atli Benediktsson. Warsaw, Poland: SPIE, Oct. 2017.

- [25] Yingchang Li et al. “Forest aboveground biomass estimation using Landsat 8 and Sentinel-1A data with machine learning algorithms”. In: *Scientific Reports* 10.1 (June 2020). ISSN: 2045-2322. DOI: 10.1038/s41598-020-67024-3. URL: <http://dx.doi.org/10.1038/s41598-020-67024-3>.
- [26] Diederik P. Kingma and Jimmy Ba. *Adam: A Method for Stochastic Optimization*. 2014. DOI: 10.48550/ARXIV.1412.6980. URL: <https://arxiv.org/abs/1412.6980>.
- [27] Maurizio Santoro and Oliver Cartus. *ESA Biomass Climate Change Initiative (Biomass\_cci): Global datasets of forest above-ground biomass for the years 2010, 2017, 2018, 2019 and 2020, v4*. en. 2023. DOI: 10.5285/AF60720C1E404A9E9D2C145D2B2EAD4E. URL: <https://catalogue.ceda.ac.uk/uuid/af60720c1e404a9e9d2c145d2b2ead4e>.

## Supplementary Material

### 7.1 Hosting, licensing, and maintenance plan

The processed, ready-for-use data is hosted on HuggingFace, where it can be easily accessed:

```
#!pip install datasets
from datasets import load_dataset
dataset = load_dataset("prs-eth/AGBD", streaming=True)["train"] # or test, val
```

The raw data, dense predictions, and model weights are hosted on the ETH Research Collection platform, guaranteeing long-term preservation. The code to reproduce all steps (training and evaluation of models, patch creation, downloading raw data) is hosted on the project’s public GitHub repository. The Croissant metadata for the dataset is available through HuggingFace.

The DOI of the dataset is 10.3929/ethz-b-000674193.

The data is available under a CC BY-NC 4.0 DEED license. You are free to copy and redistribute the material in any medium or format; remix, transform, and build upon the material. You must give appropriate credit, provide a link to the license, and indicate if changes were made. Importantly, you may not use the material for commercial purposes.

The dataset will be maintained by the authors to the best of their abilities and availability. The authors bear all responsibility in case of violation of rights.

### 7.2 Patches creation

In this section, we describe in more details the implementation of the data assembly and creation of the dataset. We refer to this step as *patch creation*, referring to its final product, square image patches.

As evidenced in Table 3, the various data sources are not aligned in terms of resolution. The first step in the patches creation process is to upsample the data sources to 10 m resolution when necessary. For the continuous variables (the 20 m and 60 m Sentinel-2 bands, the ALOS-2 PALSAR-2 bands, the ALOS DEM band, and the LC probability band) we apply bilinear interpolation. For categorical variables (the Sentinel-2 SCL band, and the LC band) we apply nearest neighbour.

Table 3: Data sources

	<b>GEDI</b>	<b>S2</b>	<b>ALOS-2 PALSAR- 2</b>	<b>ALOS DEM</b>	<b>LC</b>	<b>CH</b>
<b>Source</b>	NASA	Copernicus	JAXA	JAXA	Copernicus	Lang et al.
<b>Resolution (m)</b>	25	[10,20,60]	25	30	100	10
<b># of channels</b>	-	12	2	1	2	2
<b>Temporality</b>	-	monthly	yearly	once	once	yearly

The next step is to actually create the patches. We iterate (in parallel) over the Sentinel-2 tiles covering the regions of interest and load the GEDI footprints that fall within the tile. We then iterate over the footprints, and for each footprint, we consider all Sentinel-2 products for the tile at hand in the six months preceding the footprint acquisition, and take the closest one. For the yearly available data products, we take the tile-cropped data from the year of the footprint acquisition. For the fixed

data products (DEM and LC) we simply take the tile-cropped map. For all data sources, we crop the data to a  $25 \times 25$  pixel square centered around the footprint, which we store in a HDF5 file (the dataset hierarchy can be found in Figure 7). At extraction time, the window size of the patch is fixed ( $25 \times 25$ ) but users of the dataset can load any patch size, from pixel-wise ( $1 \times 1$ ) to the original  $25 \times 25$ , as long as the patch size is of size  $2k + 1 \times 2k + 1$  to respect the central pixel approach.

We then define a train/validation/test split. We do not perform the split at the GEDI footprint level, but at the Sentinel-2 tile level, meaning that all patches within the same tile will belong to the same split. To align with our geographical distribution and vegetation types distribution, we define a train/validation/test per region and enforce that the vegetation types distribution within each split should match the whole region's distribution. This is done through a random exploration within the space of possible combinations, where a combination is selected if its distribution is deemed sufficiently close to the original distribution; and where in the end we select the closest combination out of all the selected ones. We assign 65% of the tiles for training, 15% for validation, and the remaining 20% for testing. To which split each tile belongs can be found on our project's website, you can also download the mapping directly by running the following command: `wget "https://libdrive.ethz.ch/index.php/s/VPio6i5U1XTgir0/download?path=%2F&files=biomes_splits_to_name.pkl&downloadStartSecret=gxairgqzc" -O biomes_splits_to_name.pkl`

### 7.3 GBDT model initialization parameters

We hereby specify the initialization parameters for the GBDT models:

```
num_leaves = 165, max_depth = -1, learning_rate = 0.1, num_iterations = 1000,
min_split_gain = 0., min_child_weight = 1e-3, min_child_samples=20, reg_alpha
= 0, reg_lambda = 5, bagging_fraction = 0.5, bagging_freq = 1.
```

### 7.4 Dataset hierarchy

In Figure 7, we provide an example of how the data is structured within an .h5 file. We briefly describe each data field.

Note that in the remainder of this section, we assume that `f` is as follows: with `h5py.File('data_subset-2019-v4_5-20.h5', 'r')` as `f`:

- `S2_bands`: the Sentinel-2 L2A bands (except SCL), in their pre-processed digital number format. The order of the bands (B01, B02, B03, B04, B05, B06, B07, B08, B8A, B10, B11, B12) is stored in the attributes, and can be accessed `vif['21JXM']['S2_bands'].attrs['order']`
- `S2_bands`: the Sentinel-2 L2A Scene Classification (SCL) band. It is stored separately from the other bands for optimal memory management, as it has a different data type
- `S2_vegetation_score`: we assign a "vegetation score" to each patch, a number between 0 and 100 that represents the percentage of pixels in the patch that are vegetated
- `S2_date`: the encoded date of acquisition of the Sentinel-2 product from which the patch is extracted. The encoding is the number of days between the acquisition date and the start of the GEDI mission (`date := acquisition_date - start_of_mission`)
- `S2_pbn`: the Sentinel-2 product's Processing Baseline Number (PBN)
- `S2_ron`: the Sentinel-2 product's Relative Orbit Number (RON)
- `S2_boa_offset`: binary variable equal to 1 if the product was acquired after January 25th, 2022, and equal to 0 otherwise. This will be used by the data loader to calculate the surface reflectance values from the digital number values
- `agbd`: the reference GEDI biomass value
- `agbd`: the standard error of the reference GEDI biomass value

- `date`: the encoded date of acquisition of the GEDI footprint. Again, the encoding is the number of days between the acquisition date and the start of the GEDI mission
- `lat_offset`, `lat_decimal`, `lon_offset`, `lon_decimal`: to store the WGS84 latitude and longitude information more efficiently, we split each coordinate into its fractional (`offset`) and integral (`decimal`) parts. We store the fractional part as a single precision floating point number, and the integral part as an unsigned 8-bit integer.
- `...`: the additional GEDI features can be accessed via `f['21JXM']['GEDI'].keys()`, and a description of the features can be found in the GEDI documentation
- `ALOS_bands`: the ALOS-2 PALSAR-2 bands, in their pre-processed digital number format. The order of the bands (HH, HV) is stored in the attributes, and can be accessed via `f['21JXM']['ALOS_bands'].attrs['order']`
- `LC`: the Copernicus Land-Cover bands. The first band holds the labels, while the second one holds the corresponding class probabilities
- `DEM`: the Digital Elevation Model
- `ch`: the Canopy Height by Lang et al.
- `ch_std`: the estimated standard deviation of the Canopy Height

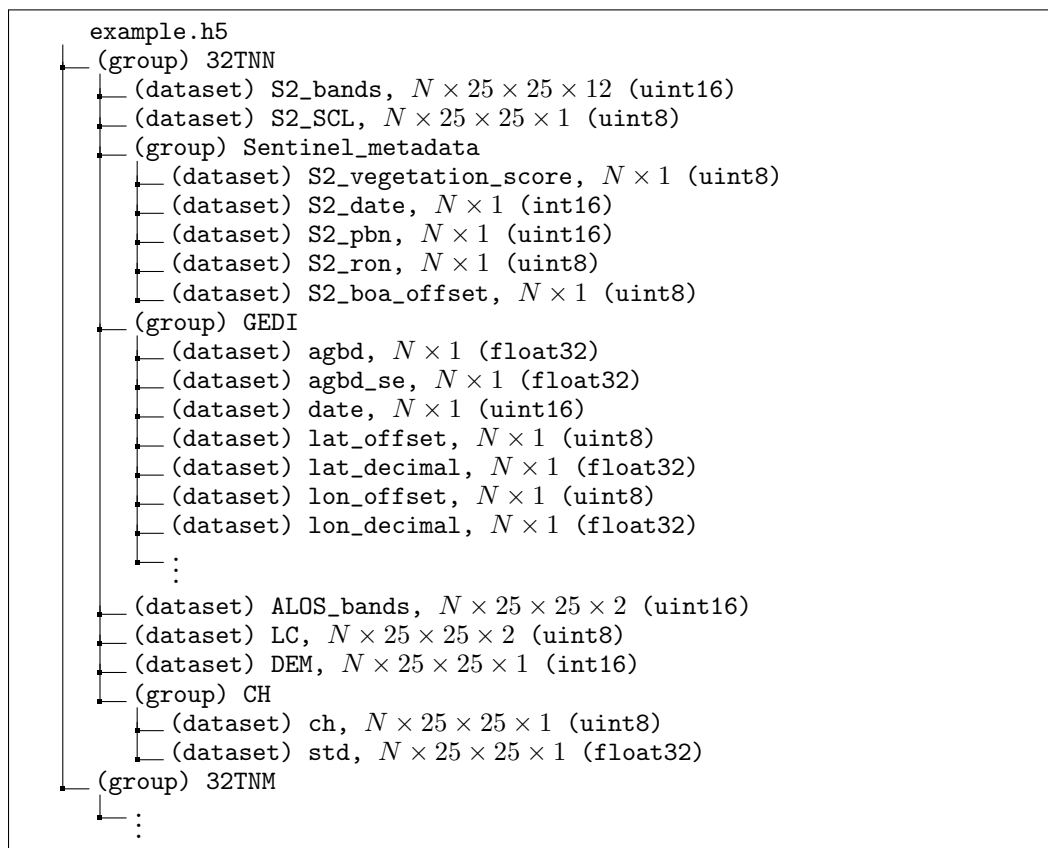


Figure 7: Sample dataset hierarchy.

## 7.5 Feature importance plots

The `lightgbm` framework provides a built-in capability to quantify the importance of each of the input features a model has access to. For each feature, it measures the total gains of splits which use the feature. We compute the feature importance for the GDBT model with all features as input, and report the corresponding plot in Figure 8.

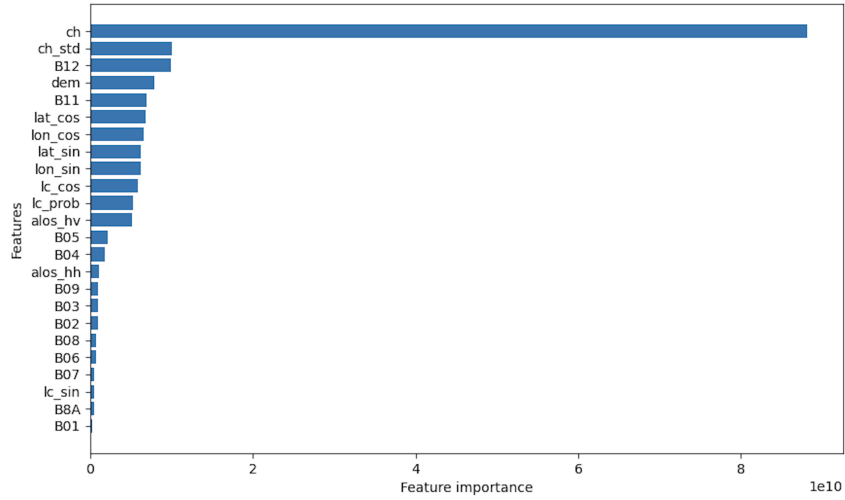


Figure 8: Feature importance for the GBDT model using all input features.

## 7.6 Confusion density plots

We further provide the confusion density plots for the best performing model of each architecture, in Figure 9. It shows good agreement between the predictions and GEDI reference, and provides insights on the distribution of the biomass values.

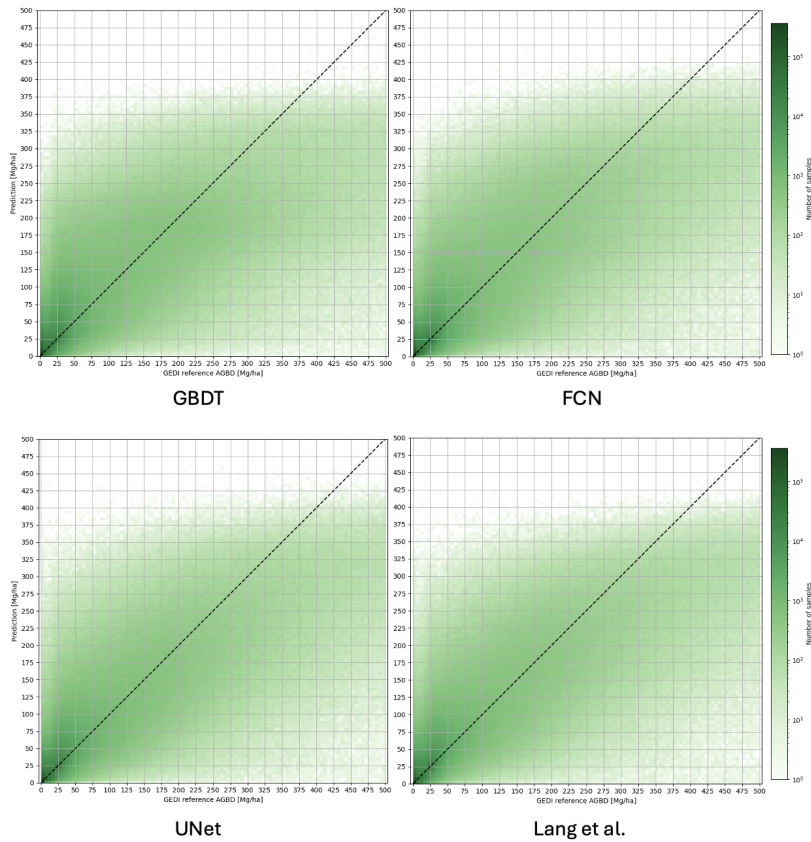


Figure 9: Density performance plots for the best model of each architecture.